Journal of Power Sources 271 (2014) 269–277

Contents lists available at ScienceDirect

Journal of Power Sources

journal homepage: www.elsevier.com/locate/jpowsour

Graphene/carbon black hybrid film for flexible and high rate performance supercapacitor

Yaming Wang [a, *], Junchen Chen [a], Jianyun Cao [a], Yan Liu [b], Yu Zhou [a], Jia-Hu Ouyang [a], Dechang Jia [a]

[a] Institute for Advanced Ceramics, Harbin Institute of Technology, Harbin 150001, China
[b] Key Laboratory of Bionic Engineering of Ministry of Education, Jilin University, Changchun 130022, China

HIGHLIGHTS

- Graphene/carbon black hybrid films were prepared by a simple vacuum filtration method.
- The supercapacitor maintained perfect rectangular shape even at high scan rate of 5 V s^{-1}.
- The supercapacitor remained 61.3% capacitance when the scan rates increased from 0.005 to 5 V s^{-1}.
- The solid-state flexible supercapacitor shows excellent rate performance and cycling stability.

GRAPHICAL ABSTRACT

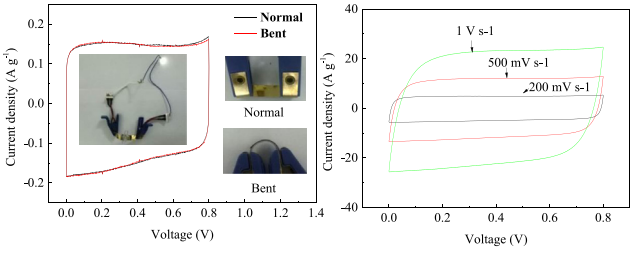

ARTICLE INFO

Article history:
Received 7 May 2014
Received in revised form
31 July 2014
Accepted 1 August 2014
Available online 11 August 2014

Keywords:
Graphene
Carbon black
Flexible
Solid-state
Supercapacitor
High rate capability

ABSTRACT

Reduced graphene oxide/carbon black (rGO/CB) hybrid films with different carbon black (CB) contents are prepared by a simple vacuum filtration method. The CB particles evenly distribute between the graphene layers, not only preventing the compact restack of rGO sheets but also providing electrical contact between the base planes of rGO sheets. As expected, the as-prepared rGO/CB hybrid film shows enhanced rate capability when compared with rGO film. Furthermore, a solid-state flexible supercapacitor has been constructed with the optimized rGO/CB hybrid film by using polyvinyl alcohol (PVA)/H_2SO_4 gel as electrolyte and Au coated PET film as current collector and mechanical support. The solid-state flexible supercapacitor shows a specific capacitance of 112 F g^{-1} at a scan rate of 5 mV s^{-1}, and excellent rate performance with a specific capacitance of 79.6 F g^{-1} at a high scan rate of 1 V s^{-1}. Moreover, the flexible solid-state supercapacitor exhibits good cycling stability with capacitance retention of 94% after 3000 cycles in normal state plus 2000 cycles in bent state.

1. Introduction

Supercapacitors, owing to its large specific capacitances when compared with conventional capacitors, long cycle life and high power delivery capability when compared with batteries, have aroused wide research interests as energy storage systems for applications in the fields of consumer electronics, hybrid electric vehicles and medical devices [1,2].

Numerous works have been accomplished to enhance the capacitance performance thus improve the energy density of supercapacitors. Owing to the high faradic pseudocapacitances, plenty of attentions have been paid to employ transition oxides and conducting polymers as electrode materials for supercapacitors.

* Corresponding author. Tel.: +86 451 86413910; fax: +86 451 86413922.
E-mail address: wangyaming@hit.edu.cn (Y. Wang).

http://dx.doi.org/10.1016/j.jpowsour.2014.08.007
0378-7753/

Among these materials, some transition metal oxides as V_2O_5 [3,4], NiO [5], TiO_2 [6], MnO_2 [7] and RuO_2 [8] have been studied extensively. Nevertheless, the poor conductivity of transition metal oxides has been a main drawback which may deteriorate the capacitance performance, rate capability and cycling stability of supercapacitors.

Recently, researchers paid more attention to the carbon/metal oxides composite materials to enhance the capacitance performance and cycling stability [9–13], such as the hybrid of MnO_2 nanowires and MWCNTs as cathode of supercapacitor has exhibited high energy density and cycling stability [14]. On the other hand, asymmetric supercapacitor in which the metal oxides or their composites serve as positive electrodes and carbon materials serve as negative electrodes can extensively broaden the working potential window, thus leading to higher energy density [12,15,16].

However, while great efforts have been devoted to develop high capacitance thus high energy supercapacitors, fewer attentions have been paid to its high power delivery capability which is the most basic requirement for supercapacitors. Moreover, as the rapid development of flexible consumer electronic products, high performance flexible electric storage devices have aroused comprehensive attentions recently.

Graphene based films, which exhibits high electrical conductivity and excellent mechanical property, are promising candidate electrode materials for flexible and high power supercapacitors [17]. To date, a lot of attempts have been concentrated on incorporating carbon nanotubes, conducting polymers and transition metal oxides with graphene to fabricate graphene based hybrid films which serve as supercapacitor electrode materials. The conducting polymers and transition metal oxides can highly improve the specific capacitance of supercapacitor, while deteriorate the rate performance rapidly [17–20]. Although the graphene/carbon nanotubes composite material can both improve the capacitance as well as rate capability [21–25], a remaining challenge is that the high prices and complicated preparation methods of carbon nanotubes seriously limit the extensive use of them in graphene based supercapacitors.

Carbon black (CB), which has high electrical conductivity and cheap price, is a good candidate to replace carbon nanotube for fabricating graphene based hybrid films. Jun Yan and his coworkers [26] have prepared rGO/CB pulverous composites by the ultrasonication and in situ reduction methods. The as-fabricated rGO/CB powder-composite electrode shows enhanced capacitance and rate capability. However, the ad-hoc nature of powder-composite electrode structure potentially restricts a high-rate response [27], and cannot fulfill the requirements of next generation wearable electronics for flexible inside energy storage devices [28].

Thus, in this work, a flexible supercapacitor with high-rate response was constructed with reduced graphene oxide/carbon black (rGO/CB) hybrid film. The rGO/CB films were prepared by a simple approach of vacuum filtration process to form unique rGO/CB hybrid gel films which are different from other earlier works on rGO/CB composite [26,36]. Fig. 1 shows the fabrication scheme of fabrication of rGO/CB hybrid gel film. The synthetic effects of rGO sheets, CB and the interlayer absorbed water lead to a large accessible surface area for the electrolyte even under high rate conditions. The optimized rGO/CB-1.5 film (with CB content of 1.5 mg per film) shows a superior rate capability with a capacitance retention of 61.3% when the scan rate increased from 5 mV s^{-1} (95.7 F g^{-1}) to as high as 5 V s^{-1} (58.7 F g^{-1}). Furthermore, we successfully constructed a solid-state device with the optimized rGO/CB-1.5 film using polyvinyl alcohol (PVA)/H_2SO_4 gel as electrolyte and Au coated PET film as current collector and mechanical support. The solid-state supercapacitor shows a specific capacitance of 112 F g^{-1} at the scan rate of 5 mV s^{-1}, and exhibits good flexibility, rate capability and excellent cycling stability.

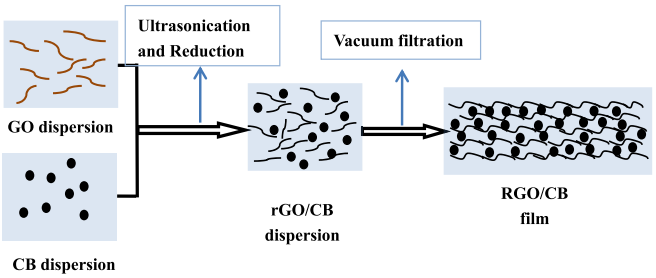

Fig. 1. Schematic of preparation of rGO/CB hybrid film.

2. Experimental

2.1. Preparation of graphene/CB hybrid film

Modified Hummers' method was used to prepare graphene oxide (GO) [29,30]. GO solid (100 mg) was mixed with 100 mL water with the aid of ultrasonication for 2 h at room temperature, and then the GO dispersion was prepared. CB (25 mg) was dispersed in 100 mL dimethylformamide (DMF) with the aid of ultrasonication for 1 h at room temperature to obtain 0.25 mg mL^{-1} of CB dispersion.

The as prepared CB dispersions with the volume of 4, 6 and 8 mL were diluted with 41, 39 and 37 mL of DMF, respectively. Then 5 mL of 1 mg mL^{-1} GO dispersion was added into the as prepared CB dispersions separately. After ultrasonication for 2 h at room temperature, the GO/CB complex dispersions with different CB contents were prepared. As a comparison, pure graphene oxide dispersion was also prepared by diluting 5 mL of 1 mg mL^{-1} GO dispersion with 45 mL DMF. Then 0.9 μL of hydrazine (50 wt% in water) was added to the as prepared complex dispersions followed with violent stir for several minutes. Then, the as prepared dispersions were reduced in water bath at 100 °C for 3 h.

The rGO/CB hybrid films were prepared by vacuum filtration of the as-synthesized rGO/CB complex dispersions through cellulose esters filter films (45 mm in diameter, 0.45 μm in pore size). During the fabrication process, vacuum filtration plays an important role in the formation of the unique rGO/CB gel film. Under vacuum filtration process, the layer by layer assembling of rGO/CB film occurs only at the interface of the membrane by filtrating excessive water from the membrane, which is regarded as a kind of sol–gel transition [37]. And the microstructure of rGO/CB gel film formed by vacuum filtration is quite different from graphene/carbon black powder in Ref. [26] and graphene/carbon black dry film in Ref. [36]. In the gel film, water also plays an important role by absorption on the surface of each graphene layer which is also crucial to prevent the restacking of graphene layers and to facilitate the ions' movement at high scan rates. The graphene film was prepared using the same procedure without adding CB was named as rGO. The rGO/CB hybrid films with different CB contents of 1 mg, 1.5 mg and 2 mg were named as rGO/CB-1, rGO/CB-1.5 and rGO/CB-2, respectively.

2.2. Characterization method

Cross section morphologies of rGO/CB hybrid films were analyzed by a scanning electron microscope (SEM, Helios Nanolab600i). X-ray photoelectron spectroscopy measurement was performed using X-ray photoelectron spectrometer (XPS, K-Alpha, Thermo Fisher Scientific Company) with monochromated Al Kα radiation ($h\nu = 1486.6$ eV). All XPS spectra were corrected using the

C1s line at 284.6 eV. Curve fitting and background subtraction were accomplished using XPS peak software.

2.3. Electrochemical measurements

The electrochemical measurement was operated by a two electrode system. The assembling steps are as follows: (1) two pieces of 1 × 1 cm^2 of rGO/CB hybrid films and a piece of 1.5 × 1.5 cm^2 of cellulose esters tilter film (0.45 μm pore size, served as separator membrane) were all soaked in 1 M H_2SO_4 for 2 h; (2) the two pieces of rGO/CB hybrid films, separated by the cellulose esters tilter film, were clamped by two pieces of pure Ti plates which worked as current collectors. Then the rGO/CB hybrid film based supercapacitor was assembled. The measurement was carried out in 1 M of H_2SO_4 aqueous electrolyte at room temperature. Cyclic voltammetry (CV) was measured by an electrochemical workstation (CHI 604C, China) at the scan rate from 0.005 V s^{-1} to 5 V s^{-1}, and galvanostatic charge/discharge was realized by a battery test system (CT2001A, China). The electrochemical impedance spectroscopy (EIS) was studied by an electrochemical workstation (M273, USA) with a frequency range of 0.01 Hz–10 KHz by applying an AC signal of 10 mV in amplitude.

3. Results and discussion

3.1. Physic-chemical characterization of graphene/CB hybrid films

Fig. 2a shows a digital photograph of free standing rGO/CB-2 hybrid film, indicating a similar flexible characteristic to rGO film. The cross section SEM images of rGO and rGO/CB hybrid films were shown in Fig. 2b–e, the insert pictures are the corresponding low magnification images. It is obvious that for the rGO film without CB, the graphene layers are restacked together (Fig. 2b). While for the rGO/CB-1, rGO/CB-1.5 and rGO/CB-2 hybrid films, the graphene layers were separated apart by CB (Fig. 2c–e), which will facilitate the electrolyte ions' diffusion between graphene layers when used as supercapacitor electrode. However, with the CB content increasing, the agglomeration of CB becomes more serious which may be disadvantageous for the enhancement specific capacitance.

XPS is widely used in the compositional analysis of materials. To investigate the compositions change of GO film before and after reduced by hydrazine, the XPS spectrum was performed on GO and rGO films. The C1s XPS spectrums of GO and rGO are shown in Fig. 3. As shown in Fig. 3a, the spectrum of GO clearly reveals four components of carbon bond, namely, C–C/C=C, C–O, C=O, O=

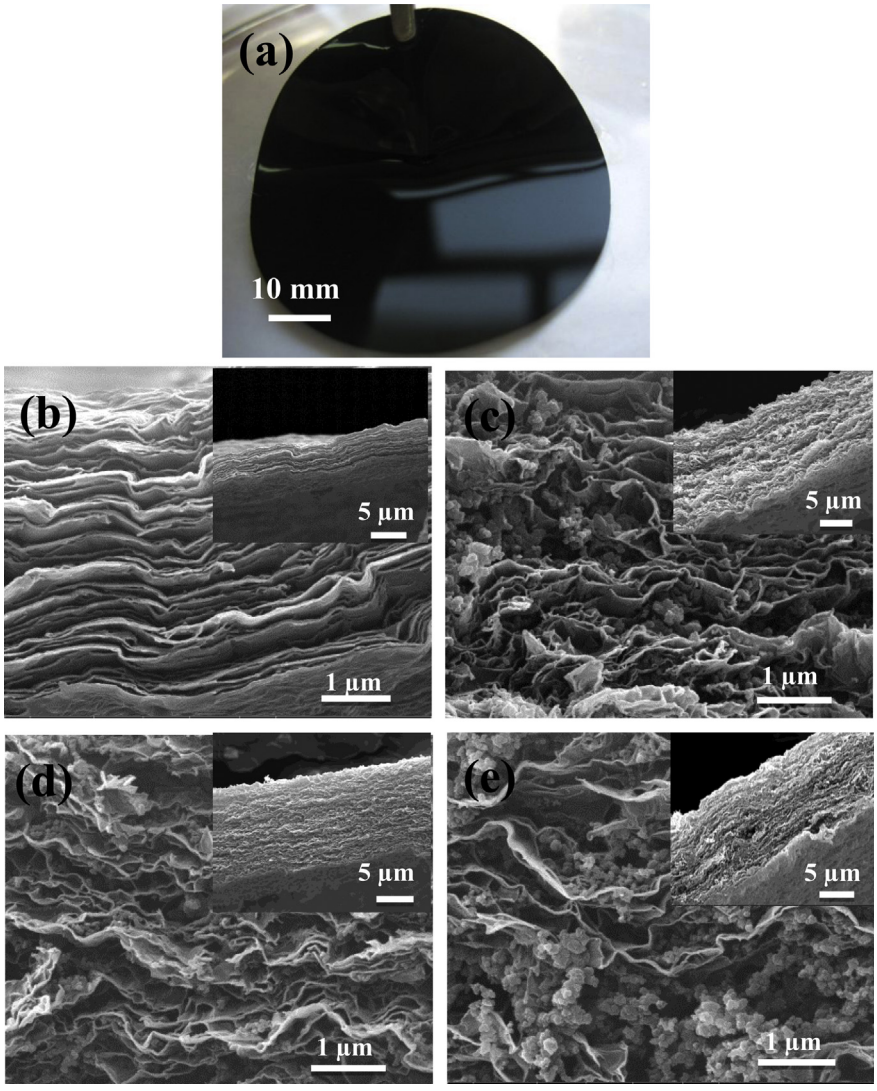

Fig. 2. (a) Digital image of rGO/CB-2; (b), (c), (d) and (e) cross section SEM images of rGO, rGO/CB-1, rGO/CB-1.5 and rGO/CB-2, respectively.

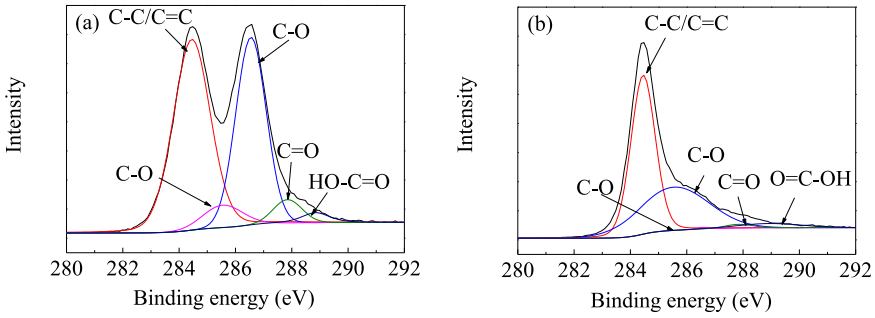

Fig. 3. XPS spectrums of GO and rGO. (a) XPS C1s spectra of GO; (b) XPS C1s spectra of rGO.

C—OH, respectively [19,32]. Compared with GO, the C—C/C=C bond of C1s XPS spectrum of rGO, as shown in Fig. 3b, becomes predominant, while the O/C atom ratio decreases from 0.40 to 0.18, demonstrating that most of the oxygen-containing functional groups have been dramatically removed after hydrazine reduction.

3.2. Electrochemical characterization of graphene/CB hybrid films

Fig. 4 shows the CV curves of rGO and rGO/CB hybrid films with different CB contents in 1 M of H_2SO_4 aqueous electrolyte at the potential range of [0, 0.8 V]. Fig. 4a shows the CV curves of rGO at the scan rates of 0.2, 1 and 5 V s^{-1}. The rectangular shape of CV curves at the scan rate of 0.2 V s^{-1} shows a typical electric double layer capacitance. For the rGO/CB hybrid films with different CB contents (Fig. 4b–d), the CV curves still maintain distinct rectangular characteristics when the scan rate increases to as high as 5 V s^{-1} illustrating excellent rate capabilities. Fig. 4e compares the CV curves of rGO and rGO/CB hybrid films at the same scan rate of 5 V s^{-1}. Particularly, at the scan rate of 5 V s^{-1}, rGO/CB-1.5 film shows the best rectangular characteristic and the largest area which means the best rate capability and highest specific capacitance in such a high scan rate of 5 V s^{-1}.

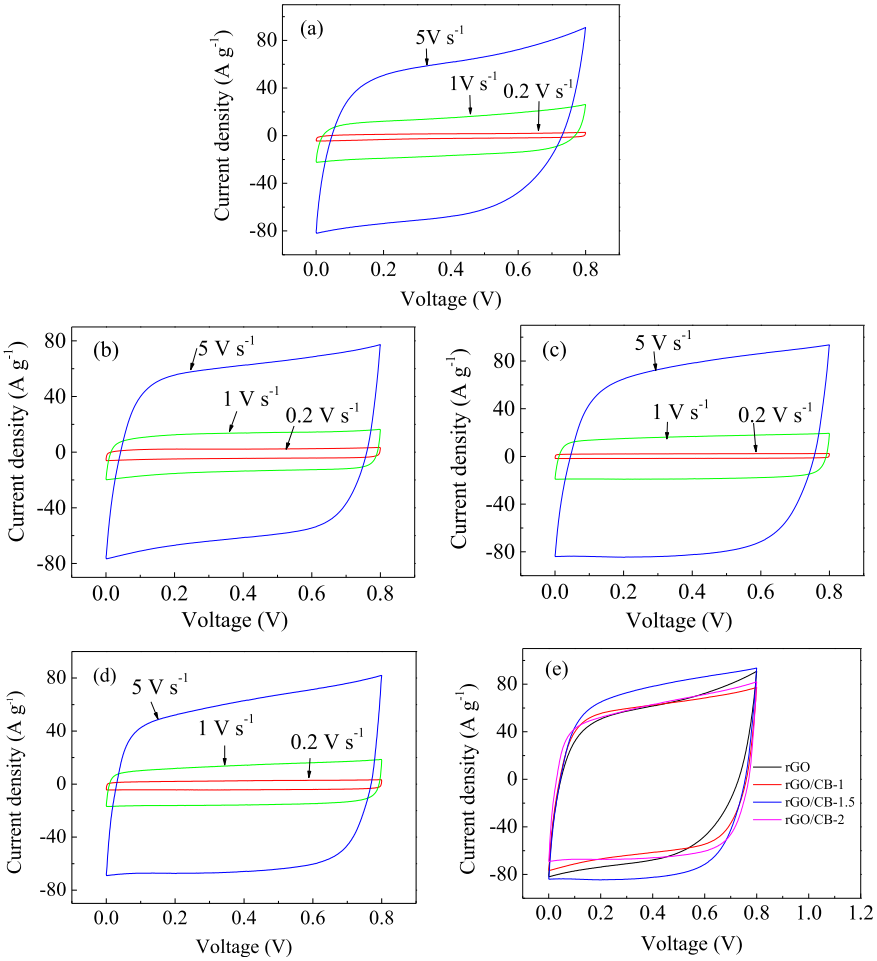

Fig. 4. CV curves of graphene based graphene/carbon black papers (the current density is obtained by normalizing the total weight of the two electrodes). (a) rGO; (b) rGO/CB-1; (c) rGO/CB-1.5; (d) rGO/CB-2; (e) CV curves of rGO, rGO/CB-1, rGO/CB-1.5 and rGO/CB-2 at the scan rate of 5 V s^{-1}.

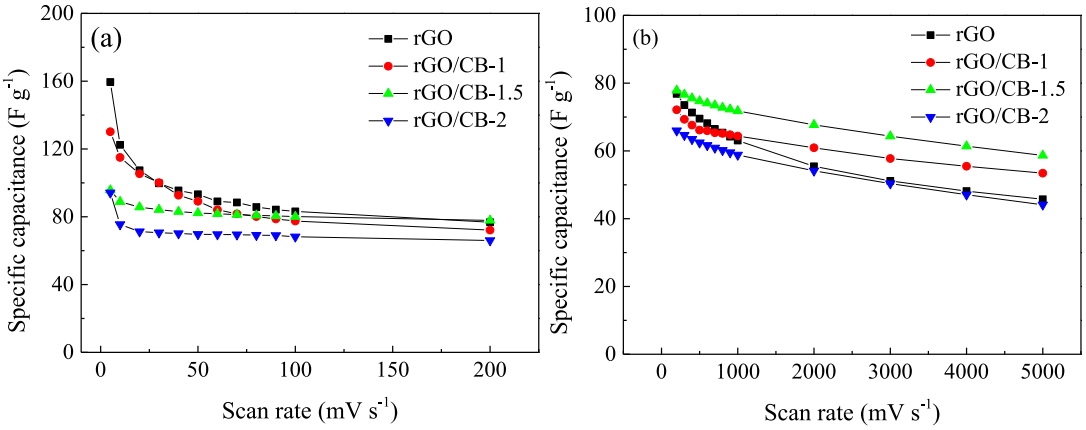

Fig. 5. Specific capacity of the graphene based films. (a) Scan rates from 0.005 to 0.1 V s^{-1}; (b) scan rates from 0.2 to 5 V s^{-1}.

The specific capacitance of graphene based hybrid films electrodes are calculated from the CV curves according to the following equation [33]:

$$C_{cell} = \frac{1}{2mv(V_2 - V_1)} \int I(v)dV \quad (1)$$

Thus:

$$C = 4C_{cell} \quad (2)$$

where C_{cell} is the specific capacitance of the whole device (F g^{-1}) and C is the specific capacitance of the single rGO/CB-1.5 film (F g^{-1}), m is the total mass of the two electrodes (g), v is the scan rate (mV s^{-1}), $V_2 - V_1$ is the sweep potential range of the CV curves [0, 0.8 V], $\int I(v)\,dV$ is the integral area of the CV curve.

The specific capacitance evolutions of the rGO/CB hybrid films based supercapacitors when the scan rate increased from 0.005 to 5 V s^{-1} are shown in Fig. 5. As is shown in Fig. 5a, with the scan rates below 0.2 V s^{-1}, the specific capacitances of the rGO/CB hybrid films decrease with the increasing of CB content. The decrease of specific capacitance at slow scan rates for our rGO/CB gel film is in contrary with the previous reported rGO/CB powder composite [26] and hybrid film [36] in dry state. The reason can be easily understood by clarifying the role of absorbed interlayer water in the rGO/CB hybrid gel film. Both the interlayer absorbed water and CB can prevent the rGO sheets from compact restacking, while the CB can provide a larger interlayer distance than water molecule due to its larger size. For the dried pure rGO powder and film, the loss of absorbed water resulted in compact restack of rGO sheets due to the strong π–π attraction, thus gave poor specific capacitances even at slow scan rates [37]. Thus the incorporation of CB into the dried rGO powder or film led to an improved specific capacitance both at slow and fast scan rates [26,36]. On the contrary, in the case of our rGO gel film, the existence of interlayer absorbed water already eliminates the compact restack of rGO, and leads to a relative high specific capacitance of 159.4 F g^{-1} at a slow scan rate of 5 mV s^{-1}. Herein, the incorporation of inert CB with small specific capacitance (only 3 F g^{-1} as reported in Ref. [38]) into the rGO gel film leads to a decrease in specific capacitance at slow scan rates.

Nevertheless, the ion diffusion route provided by the interlayer absorbed water is not fast enough to afford high speed charging/discharging process. Incorporation of highly conductive CB into rGO gel film will not only widen the ion diffusion route for high speed charging/discharging, but also provide good electrical connect between base plane of each rGO sheet. As expected, the specific capacitance of rGO film drops dramatically from 159.4 to 45 F g^{-1} when the scan rate increases from 5 mV s^{-1} to 5 V s^{-1} (only maintains 29.2% of its initial capacitance at the scan rate of 5 mV s^{-1}). While the specific capacitance of rGO/CB-1.5 still remains 58.7 F g^{-1} even at a high scan rate of 5 V s^{-1} (61.3% retention of the initial specific capacitance 95.7 F g^{-1} at the scan rate of 5 mV s^{-1}). To the best of our knowledge, such a superior rate performance of graphene based hybrid films has not been reported before.

For the further understanding of the effect of CB between the graphene layers, the impedance of rGO/CB hybrid films were measured in the frequency range from 0.01 Hz to 100 KHz with an AC perturbation of 10 mV. The Nyquist plot was shown in Fig. 6, the rGO/CB-2 displays the smallest semicircle at high frequency indicating a lower contact resistance, while the rGO displays the biggest semicircle. The Warburg curve of rGO/CB-2 and rGO/CB-1.5 at low frequency are both unnoticeable which means a short ion diffusion path of rGO/CB-2 and rGO/CB-1.5. The straight lines of rGO/CB hybrid films in low frequency are more parallel than that of rGO indicating the ideal capacitive behavior of rGO/CB hybrid films [12,34]. This means that the CB can highly improve the rate capability of the rGO/CB hybrid, while inadequate CB may not have enough capability to connect the graphene layers. In addition, as CB

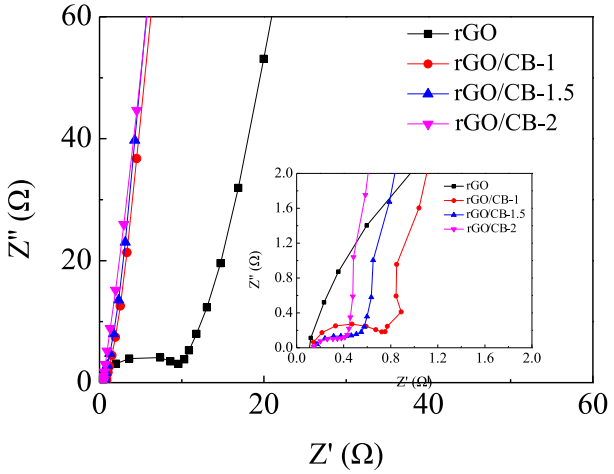

Fig. 6. Nyquist plots of rGO, rGO/CB-1, rGO/CB-1.5 and rGO/CB-2.

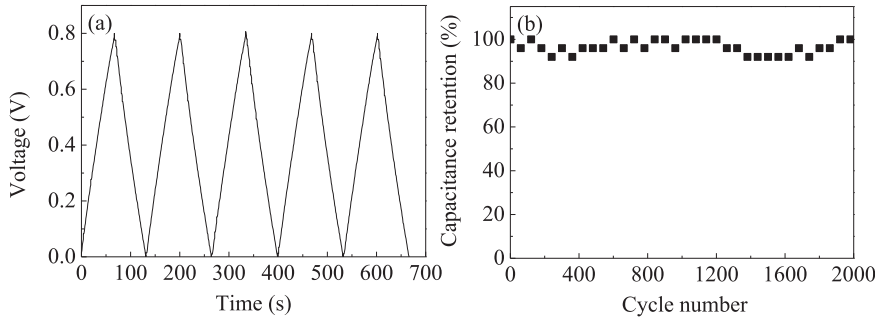

Fig. 7. (a) Galvanostatic charge–discharge curve of rGO/CB-1.5 hybrid film; (b) cycle life of rGO/CB-1.5 hybrid film.

has a low specific capacitance, overabundance of CB can bring down the total specific capacitance. Therefore, the rGO/CB-1.5 exhibits the best combination property.

Galvanostatic charge–discharge properties were performed at 0.53 A g^{-1}. The galvanostatic charge–discharge curve of rGO/CB-1.5, as shown in Fig. 7a, exhibits a triangular-shape charge–discharge curve, demonstrating that its capacitance is mainly attributed to electric double layer (EDLC) capacitance. The cycling stability of rGO/CB-1.5 is shown in Fig. 7b. After cycled for 2000 cycles, the capacitance of rGO/CB-1.5 still remained 100% of the initial capacitance, illustrating excellent cycling stability.

3.3. Solid-state supercapacitor based on rGO/CB-1.5 hybrid film

As rGO/CB-1.5 hybrid film shows the best overall performances among the rGO/CB hybrid films. Solid-state supercapacitor based on rGO/CB-1.5 hybrid film was assembled by using PVA/H_2SO_4 gel as both electrolyte and separator. The schematic of assembly of rGO/CB-1.5 based solid-state supercapacitors is shown in Fig. 8. Briefly, (1) Au film was sputtered on PET substrate (CRESSINGTON SPUTTER COATER, USA) at a current of 30 mA for 300 s; (2) Two pieces of 1 × 2 cm^2 of rGO/CB hybrid films were rolled with a glass rod onto the Au coated PET substrate individually and followed by peeling off the membrane; (3) The preparation of gel electrolyte is similar to previous publications [31,35]. PVA powder with a weight of 6 g was added into a 60 mL of 1 M H_2SO_4 solution, and then the mixture was heated to 85 °C under stirring until the solution became clear. (4) The as-prepared gel electrolyte was dripped on the electrodes, and left for15 min standing. Then two pieces of electrodes were pressed together under 0.2 MPa for 10 h. For comparison, a current collector free solid-state supercapacitor has also been assembled by using bare PET films without Au coating as mechanical support, and a piece of Ti foil was pressed at the end of each rGO/CB-1.5 film before dripping of electrolyte as wiring to the external circuit.

Firstly, the solid-state flexible supercapacitor on bare PET substrate was constructed and tested. As is shown in Fig. 9a, the CV curves of the solid-state flexible supercapacitor on bare PET substrate tested at bent state exhibits almost the same area as that tested at normal state, which illustrates negligible structural damage of rGO/CB-1.5 hybrid film at bent state. Even without current collector, the specific capacitance of the rGO/CB hybrid film is estimated to be 110 F g^{-1} at the scan rate of 5 mV s^{-1} by weighting a same area of rGO/CB hybrid film as the weight of the

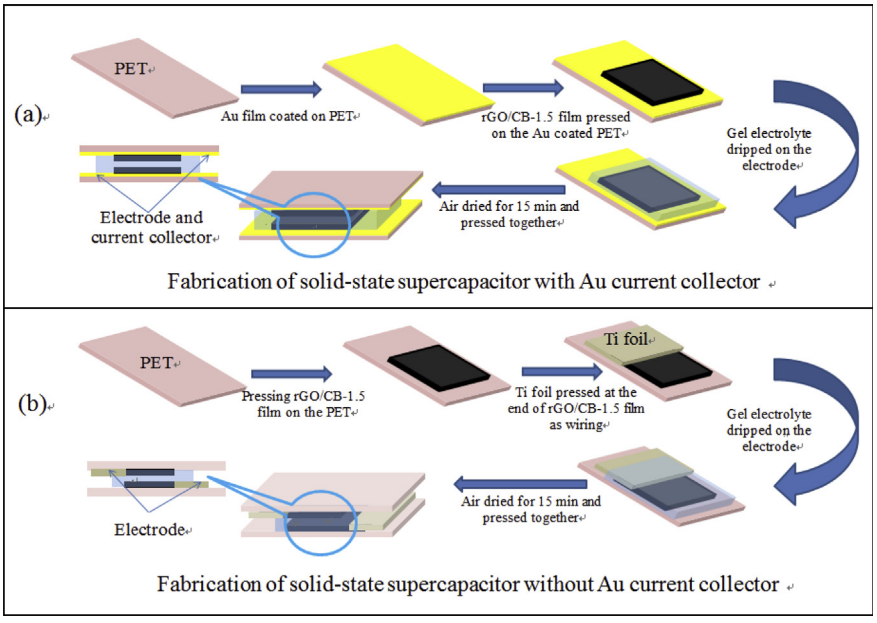

Fig. 8. Schematic of assembly of rGO/CB-1.5 based solid-state supercapacitor with (a) and without (b) Au current collector.

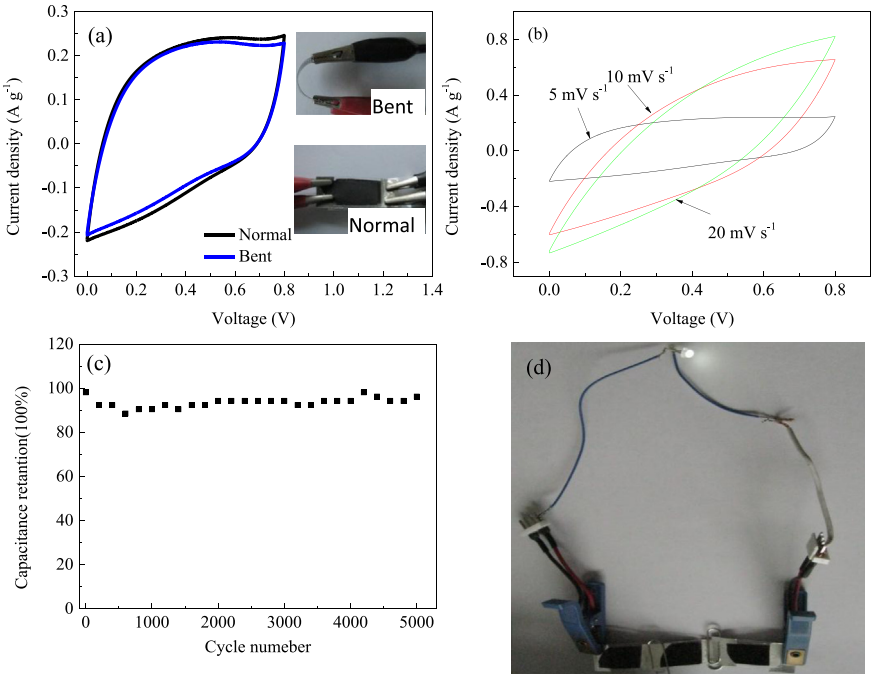

Fig. 9. (a) CV curves of solid-state supercapacitor on bare PET tested at bent and normal state (5 mV s^{-1}); (b) CV curves of solid-state supercapacitor on bare PET in different scan rates; (c) cycle life of solid-state supercapacitor on bare PET; (d) LED lightened by three solid-state supercapacitor on bare PET in series.

electrode. However, as shown in Fig. 9b, the CV curves tested in the gel electrolyte exhibit negligible rectangular characteristic even at a low scan rate of 10 mV s^{-1} which is far inferior to that tested in 1 M of H_2SO_4 aqueous solution. It is assumed that, the poor rate performance in solid-state electrolyte may be attributed to the lack of current collector and poorer mobility of ions in solid-state electrolyte. Fig. 9c shows that the capacitance maintains 96% of its initial capacitance even after 5000 cycles at the current density of 0.58 A g^{-1}, indicating that there is no considerable irreversible Faradic reaction in the solid-state flexible supercapacitor. Moreover, Fig. 9d shows a light-emitting diode (LED) lightened by three rGO/CB-1.5 hybrid film based solid-state supercapacitors in series.

To achieve a high rate performance of the solid-state flexible supercapacitor, Au coated PET was used as both substrate and current collector. Seen from Fig. 10a, CV curves of the solid-state supercapacitor on Au coated PET was tested at both bent and normal state. The CV curves highly coincide with each other, suggesting a perfect structural integrity of the solid-state supercapacitor. The CV curves of the solid-state supercapacitor on Au coated PET under different scan rates (Fig. 10b) all reveals good rectangular characteristic even at a high scan rate of 1 V s^{-1}. It means that the solid-state flexible supercapacitor based on rGO/CB-1.5 on Au coated PET substrate inherits the superior rate capability of rGO/CB-1.5 film tested in 1 M of H_2SO_4 aqueous solution. The specific capacitances of solid-state flexible supercapacitor on Au coated PET substrate at different scan rates are shown in Fig. 10c. The specific capacitance at scan rate of 5 mV s^{-1} reaches 112 F g^{-1} which is slightly higher than that on bare PET substrate. Moreover, the rate capability of solid-state supercapacitor on Au coated PET substrate is much superior than that on bare PET substrate, as the capacitance of solid-state supercapacitor on bare PET decreases to 19.6 F g^{-1} at the scan rate of 50 mV s^{-1}, while on Au coated PET its capacitance remains 79.6 F g^{-1} even at the scan rates of 1 V s^{-1} indicating that Au film, served as current collector, greatly enhanced the rate capacitance behavior of solid-state supercapacitor. Cycle life is another key parameter for the performance characterization of supercapacitor. Thus, the cycling stability was tested under current density of 2 A g^{-1} while the first 3000 cycles were tested at normal state and the last 2000 cycles were tested at bent state. As shown in Fig. 10d, after 5000 cycles, the capacitance remains 94%, demonstrating a perfect cycling stability and an excellent structural integrity at bent state. Furthermore, a LED has been lightened successfully by three rGO/CB-1.5 hybrid film based solid-state supercapacitors in series (Fig. 10e). This result indicates the potential of using the rGO/CB hybrid film to fabricate practical energy storage devices.

4. Conclusion

Flexible rGO/CB hybrid films with different CB contents were prepared by a simple vacuum filtration method. The CB existing between the graphene layers acts as spacers which prevents the restacking of graphene layers and improves the conductivity between the graphene layers. The rGO/CB-1.5 film exhibits an overall supercapacitor performances with superior rate capability as the specific capacitance maintained 61.3% when the scan rate increased from 5 mV s^{-1} (95.7 F g^{-1}) to as high as 5 V s^{-1} (58.7 F g^{-1}). The as-fabricated solid-state supercapacitor based on rGO/CB-1.5 hybrid film on Au coated PET shows a specific capacitance of 112 F g^{-1} at the scan rate of 5 mV s^{-1}, and combines good flexibility, excellent rate performance with a specific capacitance of 79.6 F g^{-1} at a high scan rate of 1 V s^{-1}), and good cycling stability with capacitance retention of 94% after 3000 cycles in normal state plus 2000 cycles in bent state. This work demonstrates the potential of using rGO/CB hybrid film to fabricate flexible, solid-state and high rate performance supercapacitors.

Acknowledgments

The partial supports from the NSFC grant nos. 51371071, 51321061 and 51275555, National Basic Science Research Program

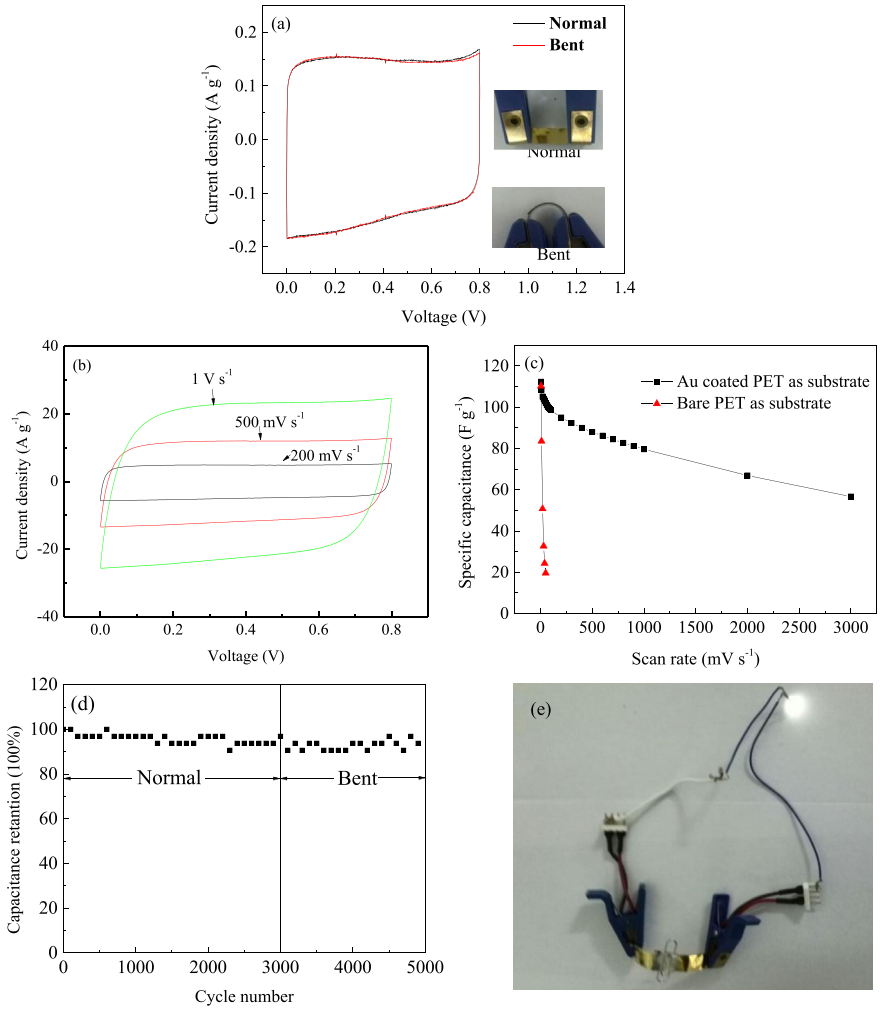

Fig. 10. (a) CV curves of solid-state supercapacitor on Au coated PET tested at bent and normal state under a scan rate of 5 mV s^{-1}; (b) CV curves of solid-state supercapacitor on Au coated PET under different scan rates; (c) specific capacitance evolution of solid-state supercapacitors with the increase of scan rates; (d) cycle life of solid-state supercapacitor on Au coated PET; (e) LED lightened by three flexible supercapacitor based on Au coated PET in series.

(2012CB933900), the Fundamental Research Funds for the Central Universities (HIT. BRETIII.201202) and the program for New Century Excellent Talents in University of China (NCET-08-0166) are gratefully acknowledged.

References

[1] K. Sahay, B. Dwivedi, J. Electric. Syst. 5 (2009) P8.
[2] I. Hadjipaschalis, A. Poullikkas, V. Efthimiou, Renew. Sustain. Energy Rev. 13 (2009) 1513–1522.
[3] W. Tang, X. Gao, Y. Zhu, Y. Yue, Y. Shi, Y. Wu, K. Zhu, J. Mater. Chem. 22 (2012) 20143–20145.
[4] Z. Chen, V. Augustyn, J. Wen, Y. Zhang, M. Shen, B. Dunn, Y. Lu, Adv. Mater. 23 (2011) 791–795.
[5] J.W. Lee, T. Ahn, J.H. Kim, J.M. Ko, J. Kim, Electrochim. Acta 56 (2011) 4849–4857.
[6] Y. Yang, D. Kim, M. Yang, P. Schmuki, Chem. Commun. 47 (2011) 7746–7748.
[7] R. Jiang, T. Huang, J. Liu, J. Zhuang, A. Yu, Electrochim. Acta 54 (2009) 3047–3052.
[8] C. Hu, K. Chang, M. Lin, Y. Wu, Nano Lett. 6 (2006) 2690–2695.
[9] J. Li, X. Wang, Q. Huang, S. Gamboa, P.J. Sebastian, J. Power Sources 160 (2006) 1501–1505.
[10] G. Wang, M. Qu, Z. Yu, R. Yuan, Mater. Chem. Phys. 105 (2007) 169–174.
[11] J. Yan, T. Wei, Z. Fan, W. Qian, M. Zhang, X. Shen, F. Wei, J. Power Sources 195 (2010) 3041–3045.
[12] Q. Qu, L. Li, S. Tian, W. Guo, Y. Wu, R. Holze, J. Power Sources 195 (2010) 2789–2794.
[13] G. Wang, L. Zhang, J. Zhang, Chem. Soc. Rev. 41 (2012) 797–828.
[14] W. Tang, Y.Y. Hou, X.J. Wang, Y. Bai, Y.S. Zhu, H. Sun, Y.B. Yue, Y.P. Wu, K. Zhu, R. Holze, J. Power Sources 197 (2012) 330–333.
[15] F. Wang, S. Xiao, Y. Hou, C. Hu, L. Liu, Y. Wu, RSC Adv. 3 (2013) 13059–13084.
[16] J. Cao, Y. Wang, Y. Zhou, D. Jia, J. Ouyang, L. Guo, J. Electroanal. Chem. 682 (2012) 23–28.
[17] X. Yan, J. Chen, J. Yang, Q. Xue, P. Miele, ACS. Appl. Mater. Interfaces 2 (2010) 2521–2529.
[18] D.W. Wang, F. Li, J. Zhao, W. Ren, Z.G. Chen, J. Tan, Z.S. Wu, I. Gentle, G.Q. Lu, H.M. Cheng, ACS Nano 3 (2009) 1745–1752.
[19] Z. Li, Y. Mi, X. Liu, S. Liu, S. Yang, J. Wang, J. Mater. Chem. 21 (2011) 14706–14711.
[20] A. Davies, P. Audette, B. Farrow, F. Hassan, Z. Chen, J. Choi, A. Yu, J. Phys. Chem. C 115 (2011) 17612–17620.
[21] D. Yu, L. Dai, J. Phys. Chem. Lett. 1 (2009) 467–470.
[22] X. Dong, B. Li, A. Wei, X. Cao, M.B. Chan-Park, H. Zhang, L. Li, W. Huang, P. Chen, Carbon 49 (2011) 2944–2949.
[23] S. Yang, K. Chang, H. Tien, Y. Lee, S. Li, Y. Wang, J. Wang, C.M. Ma, C. Hu, J. Mater. Chem. 21 (2011) 2374–2380.
[24] Y. Kim, D. Min, Langmuir 25 (2009) 11302–11306.
[25] V.C. Tung, L. Chen, M.J. Allen, J.K. Wassei, K. Nelson, R.B. Kaner, Y. Yang, Nano Lett. 9 (2009) 1949–1955.
[26] J. Yan, T. Wei, B. Shao, F. Ma, Z. Fan, M. Zhang, C. Zheng, Y. Shang, W. Qian, F. Wei, Carbon 48 (2010) 1731–1737.
[27] M.B. Sassin, C.N. Chervin, D.R. Rolison, J.W. Long, Acc. Chem. Res. 46 (2012) 1062–1074.
[28] X. Cai, M. Peng, X. Yu, Y. Fu, D. Zou, J. Mater. Chem. C 2 (2014) 1184–1200.
[29] Z. Tai, X. Yan, J. Lang, Q. Xue, J. Power Sources 199 (2012) 373–378.
[30] X. Lu, H. Dou, B. Gao, C. Yuan, S. Yang, L. Hao, L. Shen, X. Zhang, Electrochim. Acta 56 (2011) 5115–5121.
[31] Z. Weng, Y. Su, D. Wang, F. Li, J. Du, H. Cheng, Adv. Energy Mater. 1 (2011) 917–922.

[32] S. Park, J. An, I. Jung, R.D. Piner, S.J. An, X. Li, A. Velamakanni, R.S. Ruoff, Nano Lett. 9 (2009) 1593–1597.
[33] A. Yu, I. Roes, A. Davies, Z. Chen, Appl. Phys. Lett. 96 (2010) 253105.
[34] S. Biswas, L.T. Drzal, ACS Appl. Mater. Interfaces 2 (2010) 2293–2300.
[35] L. Peng, X. Peng, B. Liu, C. Wu, Y. Xie, G. Yu, Nano Lett. 13 (2013) 2151–2157.
[36] M. Wang, J. Oh, T. Ghosh, S. Hong, G. Nam, T. Hwang, J. Nam, RSC Adv. 4 (2014) 3284–3292.
[37] X. Yang, J. Zhu, L. Qiu, D. Li, Adv. Mater. 23 (2011) 2833–2838.
[38] R.N. Reddy, R.G. Reddy, J. Power Sources 124 (2003) 330–337.